AD_____

Award Number: W81XWH-12-1-0355

TITLE: Overcoming the Mechanism of Radioresistance in Neuroblastoma

PRINCIPAL INVESTIGATOR: Brian Marples PhD

CONTRACTING ORGANIZATION: William Beaumont Hospital Inc.
Royal Oak, MI 48073

REPORT DATE: June 2014

TYPE OF REPORT: Final Report

PREPARED FOR: U.S. Army Medical Research and Materiel Command
Fort Detrick, Maryland 21702-5012

DISTRIBUTION STATEMENT: Approved for Public Release;
Distribution Unlimited

The views, opinions and/or findings contained in this report are those of the author(s) and should not be construed as an official Department of the Army position, policy or decision unless so designated by other documentation.

REPORT DOCUMENTATION PAGE

Form Approved
OMB No. 0704-0188

1. REPORT DATE	**2. REPORT TYPE**	**3. DATES COVERED**
June 2014	Final Report	30 September 2012 - 30 March 2014

4. TITLE AND SUBTITLE

Overcoming the Mechanism of Radioresistance in Neuroblastoma

5a. CONTRACT NUMBER

5b. GRANT NUMBER
W81XWH-12-1-0355

5c. PROGRAM ELEMENT NUMBER

6. AUTHOR(S)

Brian Marples, PhD

E-Mail: brian.marples@beaumont.edu

5d. PROJECT NUMBER

5e. TASK NUMBER

5f. WORK UNIT NUMBER

7. PERFORMING ORGANIZATION NAME(S) AND ADDRESS(ES)

William Beaumont Hospital Inc.
Royal Oak, MI 48073

8. PERFORMING ORGANIZATION REPORT NUMBER

9. SPONSORING / MONITORING AGENCY NAME(S) AND ADDRESS(ES)
U.S. Army Medical Research and Materiel Command
Fort Detrick, Maryland 21702-5012

10. SPONSOR/MONITOR'S ACRONYM(S)

11. SPONSOR/MONITOR'S REPORT NUMBER(S)

12. DISTRIBUTION / AVAILABILITY STATEMENT
Approved for Public Release; Distribution Unlimited

13. SUPPLEMENTARY NOTES

14. ABSTRACT
Patient survival for highly aggressive advanced-stage neuroblastoma remains poor despite a multidisciplinary approach involving aggressive surgery, chemotherapy and adjuvant radiotherapy (RT). The large RT treatment volume, and concerns about the proximity of radiosensitive normal structures, restricts the tumoricidal dose of radiotherapy that can be delivered which limits the effectiveness of adjuvant RT. To address this, we delivered radiotherapy using an entirely novel treatment schedule designed to minimize normal tissue damage. The concept was to deliver 10 pulses of low-dose RT (PRT, 10 x 0.2 Gy) using a 3 minute inter-pulse interval to introduce the RT-induced damage at a level that spares tumor vasculature in order to prevent the development of treatment-induced hypoxia, since this increases tumor resistance to radiation and chemotherapy. Moreover, damage produced at this dose level evades ATM dose-dependent DNA damage detection and repair mechanisms. In vitro, a single 2 Gy dose of PRT was not inferior to SRT in any of the 4 neuroblastoma cell lines despite the prolonged delivery time. In vivo, PRT and SRT were equally effective at controlling MC-IXC and SK-N-SH subcutaneous tumors. However, significant differences in tumor volume and regrowth were evident for MYCN-amplified SK-N-BE(2) tumors between PRT and SRT at 5 days ($p=0.008$) and 21 days ($p=0.014$) post treatment, and for the entire timeframe ($p=0.006$). Endpoint criteria was reached at 43 days for SRT but 56 days after PRT ($p=0.012$). Furthermore, tumors treated with PRT demonstrated a significant increase in FDG PET maximum standardized uptake value after treatment (SUVmax=1.13 SRT, 1.79 PRT, $p=0.03$). This increase was also significant when compared to pre-treatment values for PRT (SUVmax PreTreatment=1.04, $p=0.001$). Whereas, a significant decrease in F18-FLT SUVmax was seen between PRT and SRT ($p=0.04$), indicating PRT was more tumoricidal. Quantitative immunohistochemistry identified differences in hypoxic markers (HIF1/CA-IX) and VEGF between PRT and SRT subcutaneous tumors. These data indicate that PRT may provide a new treatment regimen for MYCN-amplified neuroblastoma tumors. While the exact mechanism behind PRT is not known, changes in vascularity and cellular proliferation during treatment likely play vital roles.

15. SUBJECT TERMS
Neuroblastoma, radiotherapy, Low dose pulsed radiotherapy, animal imaging, pre-clinical animal model

16. SECURITY CLASSIFICATION OF:			**17. LIMITATION OF ABSTRACT**	**18. NUMBER OF PAGES**	**19a. NAME OF RESPONSIBLE PERSON**
a. REPORT	**b. ABSTRACT**	**c. THIS PAGE**			USAMRMC
U	U	U	UU	21	**19b. TELEPHONE NUMBER** *(include area code)*

TABLE OF CONTENTS

INTRODUCTION

Neuroblastoma is the most common extra-cranial solid tumor of early childhood characterized by variable behavior, ranging from spontaneous regression to highly aggressive disease. Advanced-stage neuroblastoma is refractory to multi-modality therapy. Resistance is related to tumor microvessel density, therapy-induced damage to tumor vasculature and related effects on angiogenic factors [1-6]. However, paradoxically, vascular damage produces localized areas of hypoxia within the tumor volume, which can transiently protect surviving tumor cells since hypoxia reduces the effectiveness of radiotherapy and restricts the effective delivery of chemotherapeutic agents. The aim of this proposal was to test the **hypothesis that these deleterious vascular effects can be overcome by using a novel radiation delivery approach.** Conventional radiation therapy (RT) schemes involve daily treatments of 1.8–2 Gy/day to exploit reoxygenation, repair, redistribution and repopulation that occur in tumors and normal tissues between the individual daily RT dose fractions. This research proposal investigated a novel delivery scheme of pulsed radiotherapy; in which the same total daily dose of radiation (2 Gy) is given as 10 individual 0.2 Gy pulses with a 3-minute inter-pulse interval between each individual 0.2 Gy pulse. The total 2 Gy dose is therefore given using a prolonged discontinuous schedule rather than as one continuous treatment used in conventional delivery. The rationale for giving pulsed treatments is that radiation-induced DNA lesions induced by pulsed radiotherapy occurs at a rate below the detection threshold of cellular repair processes in tumor cells, and thus DNA damage accumulates, causing cell death by apoptosis at the next mitosis. The hypothesis was investigated initially in subcutaneous tumors and then an orthotopic tumor model. Conventional standard radiation or pulsed radiation was given, and tumor response was monitored by non-invasive microPET/CT imaging. Tumor histology was used to investigate the underlying biological mechanisms.

BODY

SOW FOR SPECIFIC AIM #1:

Specific Aim #1 – Establish and treat subcutaneous model on neuroblastoma (Months 1-7)
Overview: The aim is to develop a subcutaneous neuroblastoma model and treat with pulsed radiotherapy and standard RT to define radiation response and determine the best cell line for the orthotopic model.

Subtask1: Establish tumor implantation for three neuroblastoma cell lines (Months 1-2)

a. Purchase and acclimatize female CB-17/SCID mice.
b. Purchase and establish growth of cell lines in vitro.
c. Establish in vivo tumors and measure tumor growth rate using calipers

Subtask2: Compare radiation schedules for subcutaneous tumors (Months 2-9)

a. Implant female CB-17/SCID mice with subcutaneous tumors from in vitro cells.
b. Treat in vivo tumors with conventional fractionated radiotherapy and pulse schedules.
c. Assess tumor growth rate using calipers.
d. MicroPET scan animals to assess RT treatment efficacy.
e. Harvest tumors and process for immunohistochemistry to assess vascular damage.
f. Analyze data set to determine effectiveness of two RT schedules against vascular injury.

OUTCOMES OF SPECIFIC AIM #1:

Subtask 1 results: These are presented as ***in vitro*** cell culture studies and ***in vivo*** tumor studies.

In vitro studies: Four neuroblastoma cell lines, SK-N-BE(2), SK-N-SH, MC-IXC, and SH-SY5Y were purchased from ATCC. SK-N-BE(2), MC-IXC, and SH-SY5Y were grown in DMEM/F12 with 10% FBS and Pen/Strep. SK-N-SH cells were grown in DMEM with 10% FBS, Pen/Strep, L-glutamine,

non-essential amino acids, and sodium pyruvate. All cell lines were grown as monolayer cultures at 37ºC in a 5% CO_2: balance air incubator.

Conventional clonogenic survival experiments were performed to assess the radiation response of singles cell *in vitro* (**Figure 1, panel A**). The clonogenic survival data showed differences in radiation sensitivity. SH-SY5Y cells exhibited an almost linear survival curve with little evidence of a shoulder. SK-N-BE(2) were the most radioresistant. A comparison at 2 Gy (**Figure 1, panel B**) demonstrated SK-N-BE(2) cells were significantly more radioresistant than SK-N-SH and MC-IXC ($p<0.02$). Survival experiments were repeated three times. SK-N-BE(2) and MC-IXC cells produced tight discrete colonies and were amenable to conducting high-resolution low-dose survival assays to define the low-dose hyper-radiosensitivity (HRS) response over the dose range 0-1 Gy. In these low-dose assays, more cells are plated per dose point and the cells are counted as they are being plated. This increases the statistical resolution of the assay. SK-N-SH cells grow as diffuse colonies and are not amendable to the high-resolution low-dose survival assay. Evidence of HRS was only detected in the SK-N-BE(2) (**Figure 2**). HRS is defined by mathematically fitting the entire low-dose survival data set with the Induced Repair Model[7, 8]. This mathematical approach demonstrated that only SK-N-BE(2) exhibited HRS as evidenced by the inflexion in the low-dose survival curve (**Figure 3A inset**).

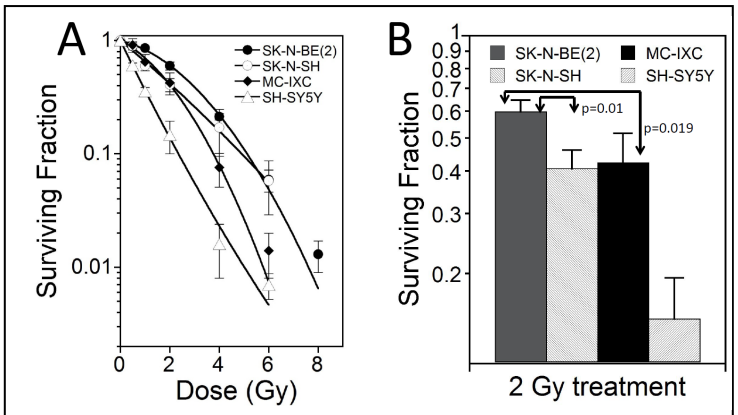

Figure 1. (A) Clonogenic survival for the four neuroblastoma cell lines (n=3, data are fitted with linear quadratic survival curve). (B) Comparison of radiosensitivity at 2Gy. SK-N-BE(2) cells are significantly more radioresistant than SK-N-SH and MC-IXC cells.

Induced Repair survival model[7, 8]: $S = \exp\left\{-\alpha_r\left(1+\left(\alpha_s/\alpha_r - 1\right)e^{-d/d_c}\right)d - \beta d^2\right\}$

Where d is dose, and αs represents the low-dose value of α (derived from the response at very low doses), αr is the value extrapolated from the conventional high-dose response, dc is the 'transition' dose point at which the change from the very low-dose HRS to the IRR response occurs (i.e. when αs to αr is 63% complete) and β is a constant as in the LQ equation[7, 8]. All parameters were fitted simultaneously and estimates of uncertainty were expressed as likelihood confidence intervals. The presence of low dose hyper-radiosensitivity is deduced by values of αs and αr whose confidence limits do not overlap and a value of dc (the change from low to high dose survival response) significantly greater than zero. The mathematic modeling using the Induced Repair model indicated that the dc value for SK-N-BE(2) cells was 0.23 Gy (StdErr=0.09 Gy) (lower confidence limit[CL]=0.02 Gy, upper confidence limit=0.54 Gy), with αs=0.901 (low CL=0.1697, upper CL=17.7429) , αr=0.1179 and β=0.029. These values compare favorably with Dc values from glioblastoma[9, 10] and prostrate cell lines [11]that show HRS. For

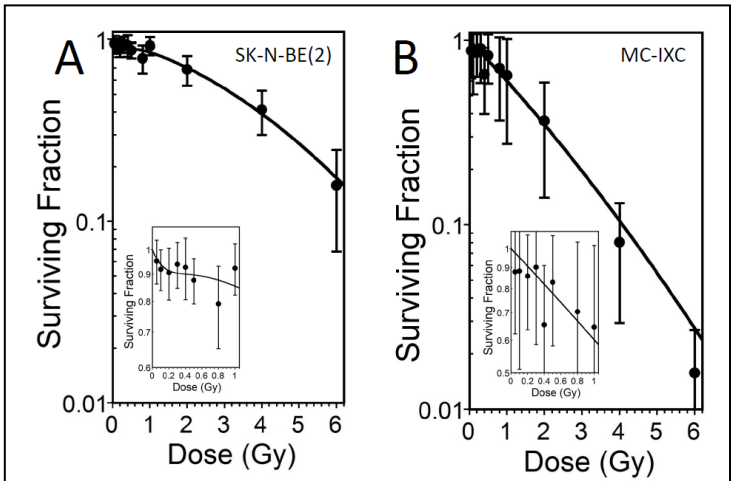

Figure 2. (A) SK-N-BE(2) (B) MC-IXC (n=3, data are fitted with Induced Repair model. Inset: Expansion of low-dose survival response over 0-1 Gy dose range.

MC-IXC cells, the confidence limits for the dc value spanned zero indicating no HRS response but a survival curve that was best described by a linear quadratic model, with α=0.473 (low CL=0.238; upper CL=0.691) and β=0.027 (lower CL=0.057; upper CL=0.203).

The radiation response of the four neuroblastoma cell lines was investigated after continuously-delivered standard radiotherapy and (SRT) and discontinuously pulsed radiotherapy (PRT) using MTT growth assay. MTT assay rather than a single-cell clonogenic assay was used as the response was determined after 5 consecutive days of treatment, with 2 Gy given per day for a 5-day total of 10 Gy. SK-N-BE(2), SK-N-SH, MC-IXC exhibited similar responses *in vitro* given by standard continuously-delivered radiotherapy (SRT) or discontinuous pulsed radiotherapy (PRT) (**Figure 3**). These assessments were made using an MTT growth assay that defines the response of a population of 400-600 neuroblastoma cells. SK-N-BE(2) and SK-N-SH exhibited similar radiation sensitivity, while MC-IXC cells were more radiosensitive. The SH-SY5Ycells were the most radiosensitive. Despite the difference in radiosensitivity of the four cell lines no significant difference in response was seen *in vitro* between SRT and PRT using the MTT assay. However, a significant difference was detected between SRT and PET in the repair of radiation-induced DNA double strand breaks (assayed by staining for γH2AX) for SK-N-BE(2) cells (**Figure 4**). The lower levels of γH2AX staining at 10 (p=0.023) and 30 minutes (p=0.041) post radiation (RT) indicate less DNA break recognition after PRT compared with SRT. These data support the hypothesis that the efficacy of PRT is due to the evasion of damage response pathways associated with low-dose hyper-radiosensitivity as originally proposed in glioblastoma ([12-15]). HRS occurs because X-ray doses less than ~0.25 Gy produce insufficient numbers of DNA double strand breaks (DSB) to fully activate a protective ATM-dependent early G2-phase cell cycle checkpoint. Failure to activate this radioprotective checkpoint means that proliferating G2-phase cells enter mitosis with unrepaired DNA DSBs and die by post-mitotic apoptosis[7, 16, 17]. Whereas, radiation doses >0.25Gy produce sufficient DNA DSBs to activate the ATM-dependent early G2-phase cell cycle checkpoint and DNA damage is repaired before cells enter mitosis. This effect was not seen in MX-IXC cells than did not exhibit HRS in the single dose survival response.

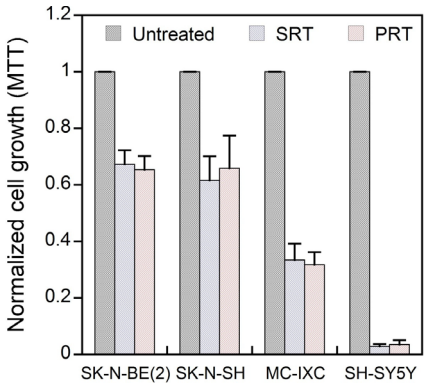

Figure 3: Measurement of cellular radiation response as assessed by MTT assay. SRT=continuous 2 Gy. PRT= discontinuously delivered 10x0.2 Gy; 3 min pulse interval.

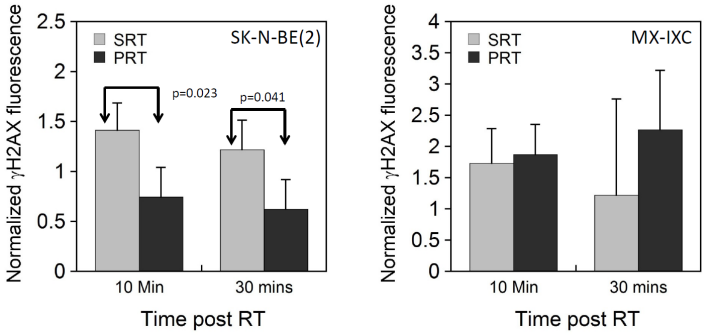

Figure 4: Normalized γH2AX fluorescence as a function of time post irradiation. Cells were irradiated *in vitro* and harvested 10 or 30 minutes following irradiation, fixed and stained with antibody specific for phosphorylated serine139 H2AX as a measure of DNA double strand breaks. Fluorescence was assay by flow cytometry to examine 20,000 cells and normalized against an unirradiated cell population. (N=3, mean±SD)

Given this *in vitro*, we established subcutaneous tumors in athymic CB-17/SCID mice with either SK-N-BE(2), SK-N-SH and MC-IXC cells; and orthotopic tumors using SK-N-BE(2) cells.

In vivo studies: Female CB-17/SCID mice were purchased from Charles River Laboratories and implanted in the rear flank with either 2x10e6 SK-N-BE(2), SK-N-SH, or MC-IXC cells in 100µL Matrigel. Each neuroblastoma cell line was implanted serially. SK-N-BE(2) tumors were established and irradiated, and then experiments with SK-N-SH and then MC-IXC tumors followed. This methodological approach extended the time needed to generate the data but was undertaken due to the limitations of PET/CT scanning. We are limited to a maximum of 5 animals per day. Each experimental group consisted of a minimum n=10 animals and each animal was scanned at least 4-5 times during and post treatment. Each group also received a pre-radiation and post radiation scan.

No difference in radiation response was seen between PRT and SRT for SK-N-SH or MC-IXC tumors (**Figure 5**). Tumors were established and irradiated daily for 10 consecutive days with either SRT (continuously-delivered dose of 2 Gy), PRT (discontinuously-delivered 10 pulses of 0.2 Gy with 3 minute inter-pulse interval) or sham-treated (no radiation, untreated controls). Irradiation was initiated when tumors reached a starting volume of 200-300 mm^3. Tumor volume was determined by physical caliper measurements twice-weekly until animals reached sacrifice criteria, either tumor volume exceeded 10% of body weight or 20% loss of starting body weight was reached. Animals with untreated naïve SK-N-SH tumors were sacrificed within 10 days for sham-treatment, and MC-IXC tumors within 20 days. SK-N-SH tumors regrew more rapidly (~35 days) after irradiation than MC-IXC tumors (~117 days). This was expected as the MC-IXC tumor cells are more radiation sensitive as determined by clonogenic survival.

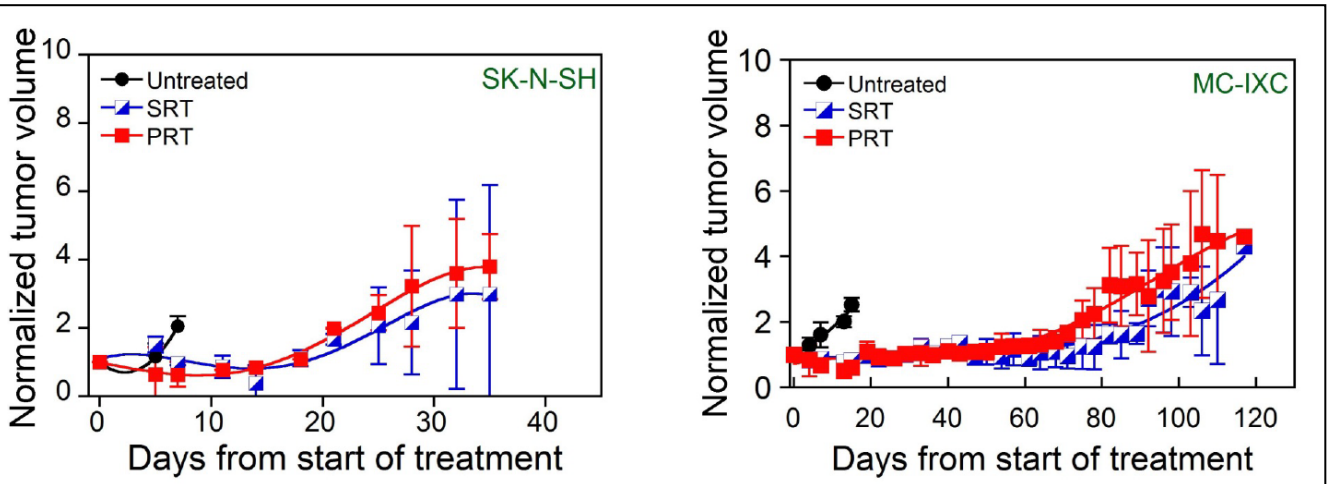

Figure 5: Normalized tumor volume as a function of days from start of treatment. No difference in response was seen between PRT and SRT (n=3, mean±SD)

However, a **statistically significant** difference in tumor response was evident between SRT and PRT for SK-N-BE(2) subcutaneous tumors ($p<0.001$, **Figure 6**). SK-N-BE(2) tumor cells exhibited HRS. PRT produced a rapid and prolonged reduction in tumor volume and tumor volume was slow to regrow. SRT produced a reduction in growth rate compared with untreated tumors but this was less effective than PRT. This effect is more evidence when the actual tumor volume is plotted (**Figure 7**). Tumor volume reached a nadir at 20 days from the start of treatment. Area under the curve (AUC) analysis indicates a significant difference in tumor response between SRT and PRT ($p=0.006$).

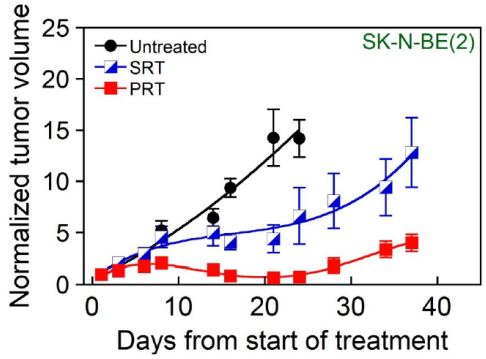

Figure 6: Normalized tumor volume as a function of days from start of treatment. A statistically significant difference in response was seen between PRT and SRT (n=7-8, mean±SD).

The data in Figure 6 are compiled from two entirely independent experiments, each consisting of n=4 animals per treatment group. PRT was more effective in SRT in both independent experiments. Comparing normalized tumor response at 2-fold and 4-fold produced statistically significant differences in experiment I (2 fold p=0.02, 4-fold p<0.01) and experiment II. (2 fold p=0.01, 4-fold p<0.001).

These data are shown as absolute tumor volume in **Figure 7**. A greater nadir of tumor response is evident after PRT than SRT (AUC p=0.0017). Tumor proliferative response after irradiation can be detected non-invasively with [F-18]FLT (3'-deoxy-3'-fluorothymidine) positron emission tomography (PET) imaging. F18-FLT provides a measure of proliferation and low levels of F18-FLT after irradiation indicates a lower proliferative response, this can be interpreted to indicate a more effective therapy regimen since few cells survival treatment to produce a large proliferative response. **Figure 8** indicates that no significant change in Mean SUVmax for untreated neuroblastoma tumors. However, the decrease in Mean SUVmax was evident 1 day after SRT and PRT irradiation. F18-FLT Mean SUVmax increased with longer times post treatment for SRT and PRT indicating tumor regrowth. Statistically significant difference were seen between day 1 and day 10 (p=0.02), 10-20 days (p=0.04) for SRT and between days 1-20 (p=0.01) for PRT. At day 20, a significant difference in response was evident between SRT and PRT (p=0.04). These data demonstrate PRT reduced the proliferative capacity of the tumor more than SRT, which is ***indicative of PRT being more effective than SRT at reducing the growth of SK-N-BE(2) tumors***.

No difference in F18-FDG PET imaging was seen for subcutaneous SK-N-BE(2) tumors (Pre-TX: **Figure 9**). 1 day post treatment, a higher Mean SUVmax was evident after PRT compared with SRT (p=0.001). F18-FDG measures tumor cell metabolism, and these data indicate a higher metabolic activity after PRT which could be considered contradictory to the F18-FLT data (indicating lower proliferative activity which tends to suggest fewer cells in the tumor). However, the F18-FDG images (see below) and harvested tumors suggested that the higher F18-FDG values simply reflected an increased uptake of the radiotracer into the tumor mass due to the absence of tumor cells. The pooling of the radiotracer in the tumor produced the higher SUVmax readings (FDG **Figure 10**, FLT **Figure 11and Figure 12**).

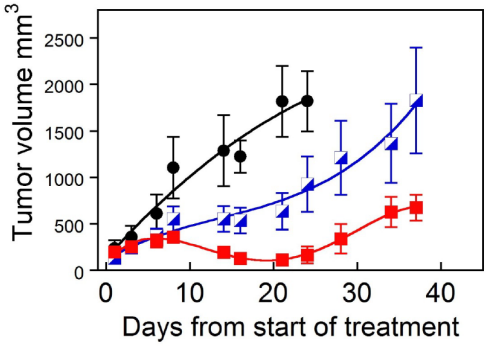

Figure 7: Tumor volume as a function of days from start of treatment for SK-N-BE(2) subcutaneous tumors. A statistically significant difference in response was seen between PRT and SRT (n=7-8, mean±SD).

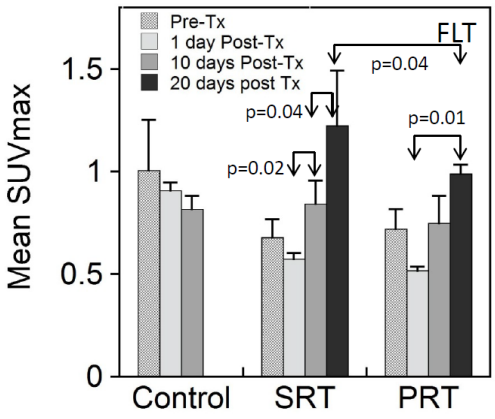

Figure 8: Mean SUVmax for F18-**FLT** imaging in animals treated with SRT or PRT (n=4, mean±SD). SK-N-BE(2) subcutaneous tumors.

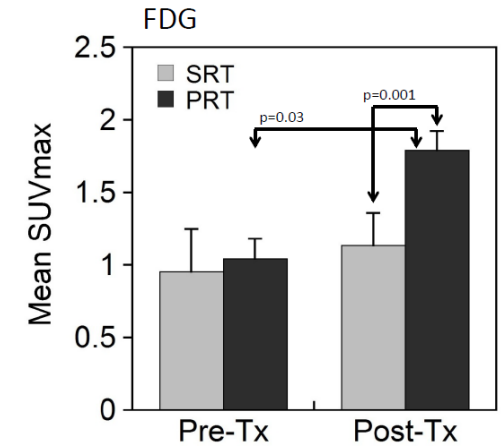

Figure 9: Mean SUVmax for F18-**FDG** imaging in animals treated with SRT or PRT (n=4, mean±SD). SK-N-BE(2) subcutaneous tumors.

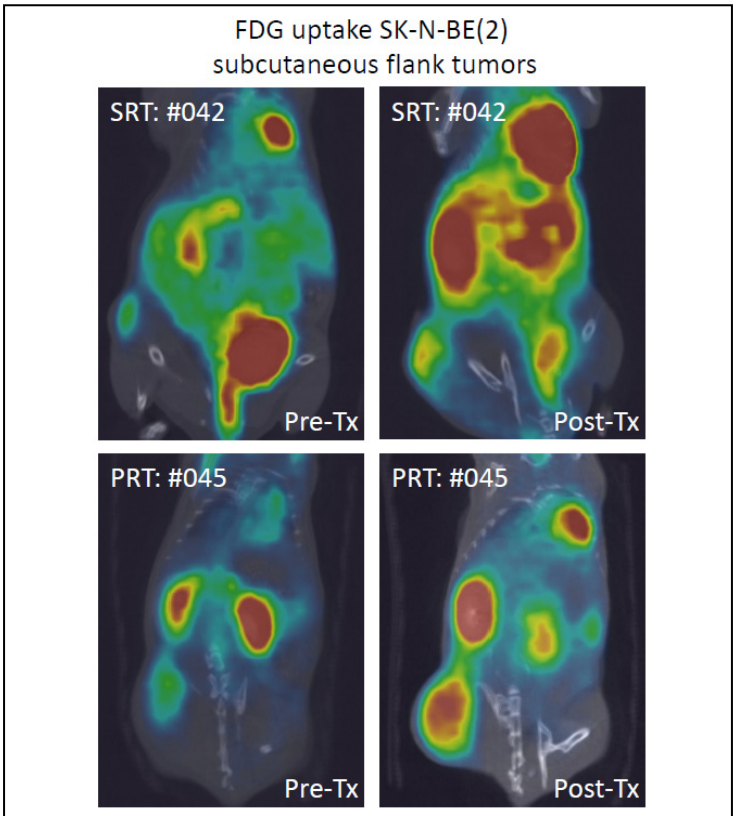

Figure 10: Representative F18-**FDG** images for individual animals treated with SRT (#042) or PRT (#045) SK-N-BE(2) to the subcutaneous tumors. Upper panels: SRT pre-treatment (pre-Tx) and 1 day post treatment (post Tx). Lower panels: PRT pre-treatment (pre-Tx) and 1 day post treatment (post Tx). Higher levels of FDG are evident post treatment after PRT. Tumor is visible on left rear flank.

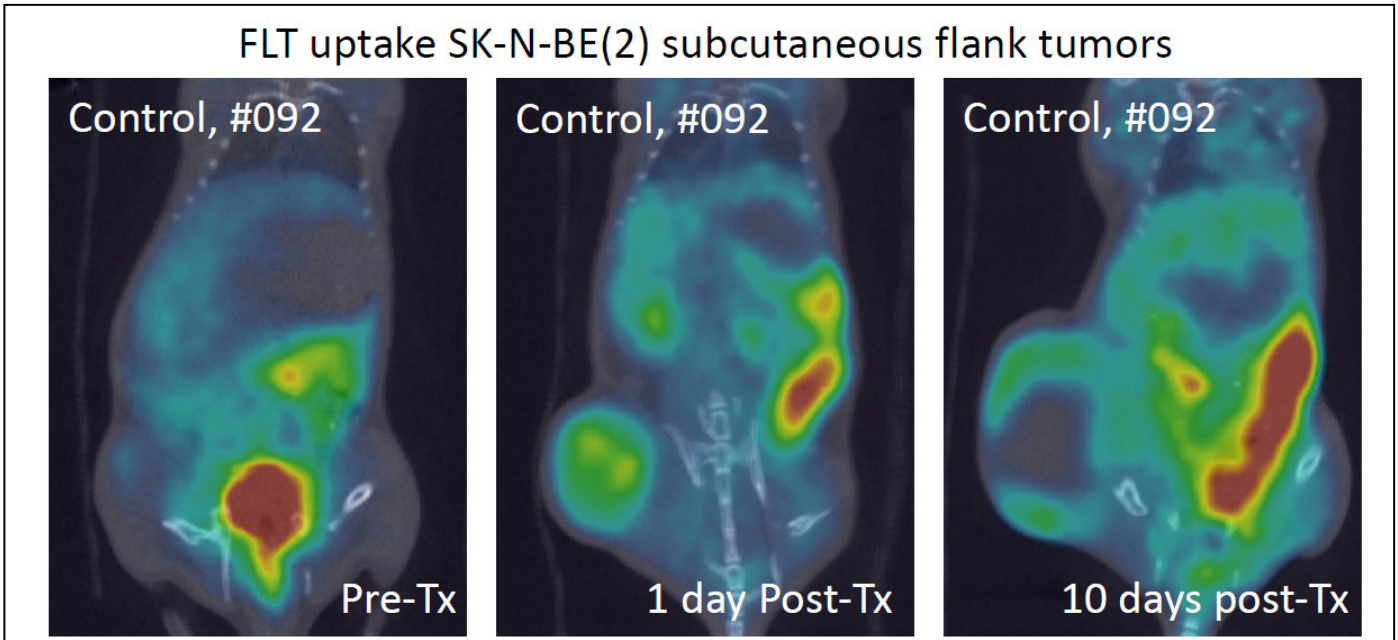

Figure 11: Representative F18-**FLT** images for an individual non-irradiated animal Pre-treatment, 1 days after sham-treatment and 10 days post treatment. FLT activity increased over the first 12 days (pre-treatment to 1 day post sham-treatment to indicate an actively proliferating tumor. Measured FLT activity reduced over the next 10 days are tumor burden increased and growth rate was reduced by metabolic constrains to tumor size. Tumor is visible on left rear flank. SUVmax quantified for multiple animals in Figure 8.

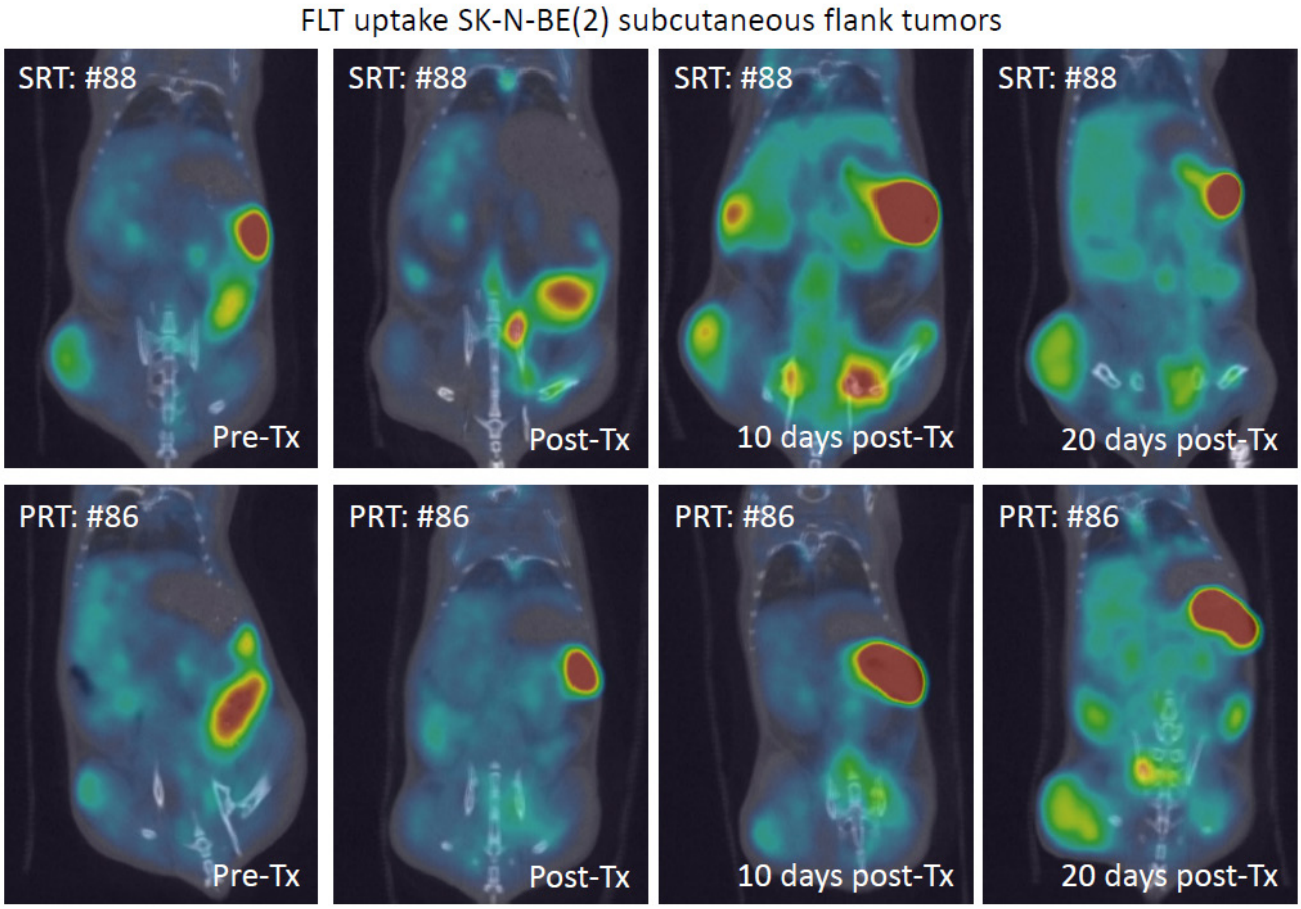

Figure 12: Representative F18-**FLT** images for individual animals treated with PRT (animal #86) and SRT (animal #88). Tumor is visible on left rear flank. Images show sequential images taken Pre-treatment (Pre-Tx) , 1 days after treatment, 10 and 20 days post treatment. FLT activity increased over the first 12 days (pre-treatment to 1 day post sham-treatment to indicate an actively proliferating tumor. Measured FLT activity reduced over the next 10 days are tumor burden increased and growth rate was reduced by metabolic constraints to tumor size. SUVmax quantified for multiple animals in Figure 8.

Similar non-invasive PET imaging studies were performed with the more slowly-growing subcutaneous MC-IXC tumors (**Figure 13**). These experiments did not indicate any differences in F18-FDG patterns after PRT and SRT. These imaging results are consistent with the tumor growth data that showed differences in response between PRT and SRT.

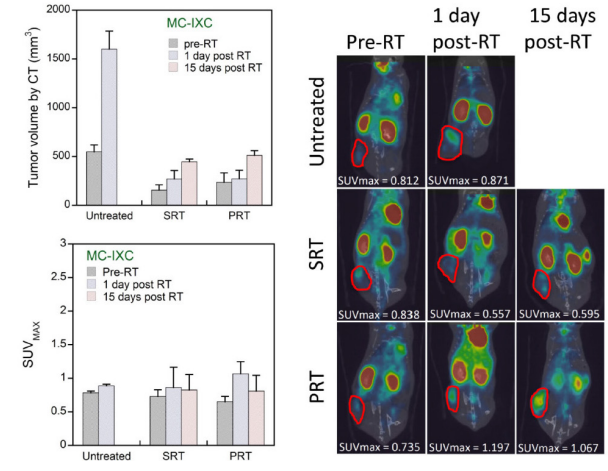

Figure 13: Mean SUVmax for F18-**FDG** imaging in animals treated with SRT or PRT (n=4, mean±SD). MX-IXC subcutaneous tumors (red circles).

The FLT imaging data, indicating differences in tumor proliferation, were confirmed by Ki67 tumor immunohistochemistry. Ki67 is a marker of proliferating S-phase cells. Subcutaneous tumors were excised after the end of treatment and other tumors excised after a regrowth period when the tumors reached sacrifice criteria. **Figure 14** demonstrates no statistically significant differences in Ki-67 after regrowth (at sacrifice), but differences for PRT between end of treatment and regrowth. There is evidence for an increase in Ki67 staining at the end of treatment for PRT compared with controls, but not for SRT. The data were obtained using Definiens Imaging software. This program uses a threshold to define positive and negative staining and then automatically, with bias from a scorer, determines the positivity across the entire tumor section (**Figure 15**). Scoring was performed in a blinded-fashion.

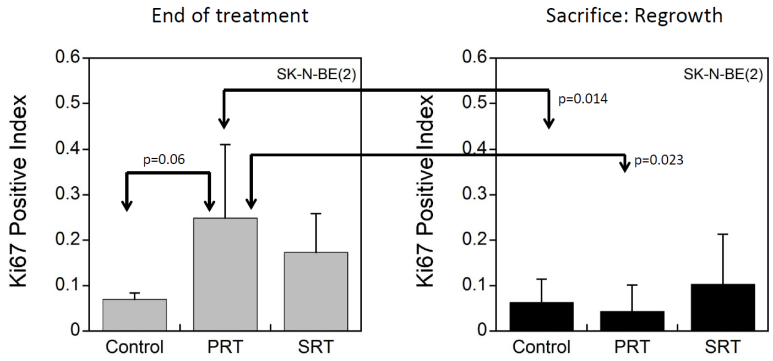

Figure 14: Percent Ki-67 staining for control and irradiated SK-N-BE(2) subcutaneous tumors. Significant differences were seen between end of treatment and sacrifice tumors for PRT. (n=7, mean±SD)

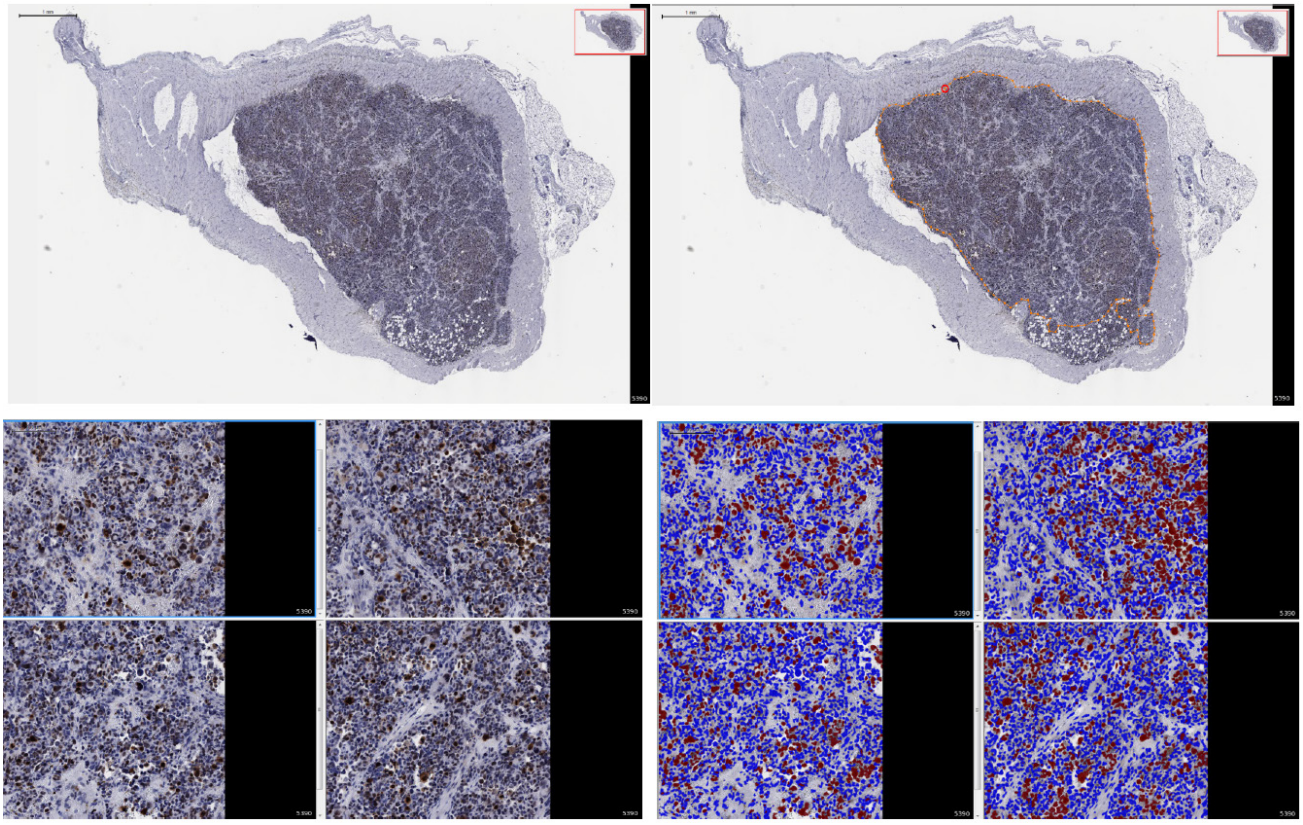

Figure 15: Top Left. Whole tumor section. Top Right: Viable tumor identified by red border. Bottom Left: Four representative sections showing positive Ki-67 staining (brown). Bottom right: Definiens mask to define the number of positive nuclei (brown stained) as a percent of all nuclei. Quantified for multiple animals in Figure 13.

Studies were conducted to determine the underlying mechanism of the increased PRT effectiveness in SK-N-BE(2) tumors. Immunohistochemistry was conducted for several hypoxia and signaling proteins (Figure 16). The data indicated significant differences in CA9 (p=0.023) and GLUT1 (p=0.047), biomarkers of tumor hypoxia. The most significant differences was evident vascular endothelial growth factor (VEGF) expression (p<0.01). The VEGF was investigated further in tumors at the end of treatment and after regrowth when tumor sacrifice criteria were met (**Figure 17**). These data confirmed that VEGF has a likely role in the effectiveness of PRT irradiation. The level of baseline and radiation-induced vascular endothelial growth factor (VEGF) expression was then measured in cell culture by ELISA assay. These data confirmed an association between lower levels of radiation-induced VEGF expression and response to PRT; linking vascular biology to PRT effects. The data presented in **Figure 18** demonstrate SK-N-BE(2) cells have low levels of radiation-induced VEGF expression, unlike SK-N-SH and MC-IXC cells that show more significant production of VEGF after radiation, given either as PRT or SRT, and that the extent of VEGF corresponds to tumor response after PRT. However, the fold increase in VEGF expression was not related to baseline levels of VEGF, since no relation was evident between baseline VEGF (**Figure 18: left panel**) and radiation response (**Figure 18: right Panel**). The reduction in E-selection may indicate a reduced metastatic potential, since the role of E-selectin has been linked with metastases in this tumor model.

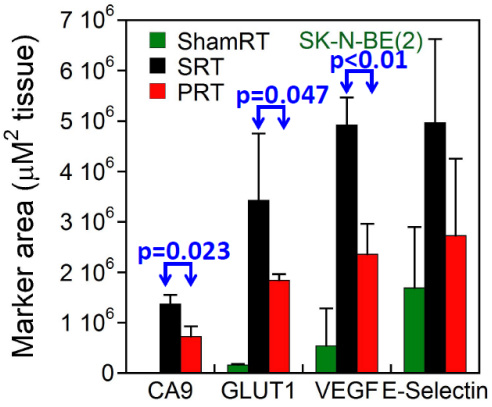

Figure 16: Definiens analysis of CA9, GLUT1, VEGF and E-selectin by antibody-specific immunohistochemistry in SK-N-BE(2) tumor sections. Sham-treated and PRT and SRT irradiated tumors.

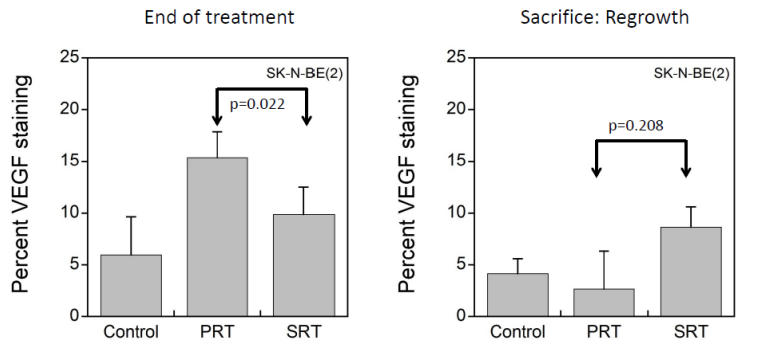

Figure 17: Definiens analysis for VEGF expression at end of treatment and after regrowth. (Mean±SD, n=7)

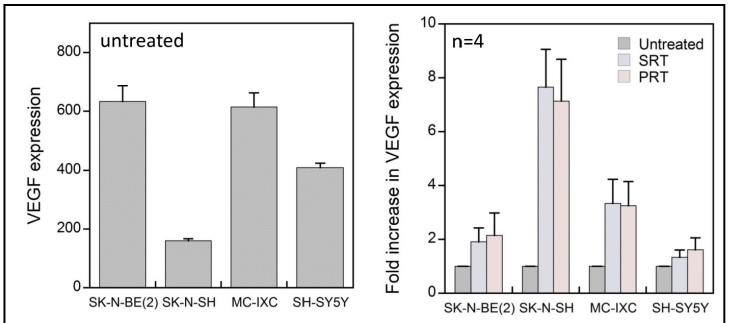

Figure 18. VEGF expression levels as assayed by ELISA. **Left** panel: The four cell lines exhibited different basal levels of VEGF expression. **Right** panel: The cell lines that showed no difference in tumor response between SRT and PRT had high levels of radiation-induced VEGF expression. SK-N-BE(2) responded differently to SRT and PRT and exhibit a non-significant increase in VEGF expression after radiation treatment.

In summary, the subcutaneous tumor response data for SK-N-SH and MC-IXC are shown in Figure 5, no difference in tumor response was seen between SRT and PRT. However, a **statistically significant** difference in tumor response was evident between SRT and PRT for SK-N-BE(2) subcutaneous tumors ($p<0.001$, Figure 6 and 7).

Aim 1 - Subtask 1 and subtask 2 were completed successfully.

These data demonstrated that PRT was more effective than SRT for rapidly-growing SK-N-BE(2) subcutaneous tumors. The effectiveness of PRT was associated with radiation-induced VEGF expression.

SOW FOR SPECIFIC AIM #2:

Overview: The aim is to develop an orthotopic neuroblastoma model and treat with pulsed radiotherapy and standard RT to define radiation response and determine treatment efficacy.

Subtask1: Establish surgical procedure for orthotopic tumor implantation (Months 7-12)

a. Purchase and acclimatize female CB-17/SCID mice.
b. Growth cell lines in vitro.
c. Establish surgical technique for orthotopic tumor implant.
d. Measure growth rate using microPET/CT.
e. Excise tumor and normal tissues for histology.
f. Compare tumor cells, normal cells and vessel density in histopathology sections.

Subtask2: Compare radiation schedules for orthotopic tumors (Months 9-18)

g. Implant female CB-17/SCID mice with orthotopic tumors from in vitro cells.
h. Treat animals with conventional fractionated radiotherapy and pulse schedules using image-guided irradiator and treated with chemotherapy.
i. Assess tumor growth rate using microPET/CT.
j. Harvest tumors and surrounding normal tissues and process for immunohistochemistry to assess vascular damage.
k. Analyze data sets to determine effectiveness of two RT schedules against vascular injury.

OUTCOMES OF SPECIFIC AIM #2:

Given the success of the SK-N-BE(2) cells as a subcutaneous model, this cell line was used to establish an orthotopic neuroblastoma model (**Figure 19**). Orthotopically, these tumors grew more quickly than the subcutaneous flank implants. Tumors were evident orthotopically with 14 days, whereas > 21 days are required before a similar sized palpable tumor is evident in the subcutaneous model.

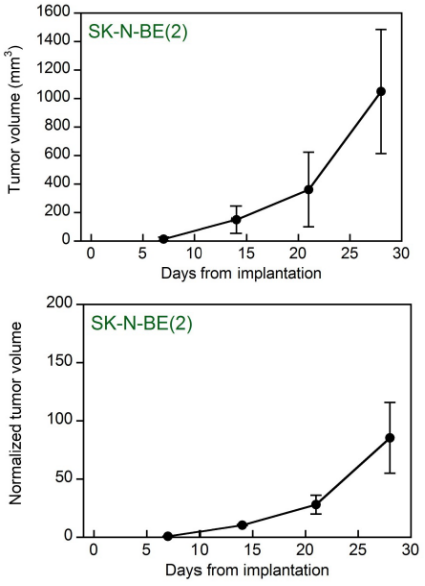

Figure 19: Growth curves of orthotopic SK-N-BE(2) tumors. N=4.

These orthotopic SK-N-BE(2) neuroblastoma tumors demonstrated similar pathology to the flank tumors.

Having defined the growth rate of the orthotopic tumors and established the model (Aim #2, Subtask1), additional animals were implanted and tumors monitored by non-invasive imaging and irradiated (**Figure 20-22**). The orthotopic tumors were irradiated using a small animal radiation research platform. This is a CT-image guided irradiation device and uses iso-center beam irradiation (**Figure 20**). The orthotopic tumor model was more variable than the subcutaneous model and therefore less reproducible. With subcutaneous tumors, all animals reached sacrifice criteria with respect to tumor burden. This was not the case with orthotopic tumors. Tumor location was a large variable and growth location affected animal health more than the subcutaneous model; this required early sacrifice due to adverse animal health in some animals (atypical posture, restricted mobility, lack of exploratory behavior consistent with species, behavior inconsistent with cage mates). Some orthotopically implanted animals were irradiated and tumor volume decreased. For example, tumor volume as assessed by T2W MRI imaging indicated average tumor volume on day 1 of 115mm^3 and 352mm^3 on day 7. 10 Gy irradiation was given on day 10. On day 14 the average tumor volume had increased to 480 mm^3, but by day 21, average tumor volume decreased to 332mm^3. These changes can be seen for a representative animal in **Figure 23**.

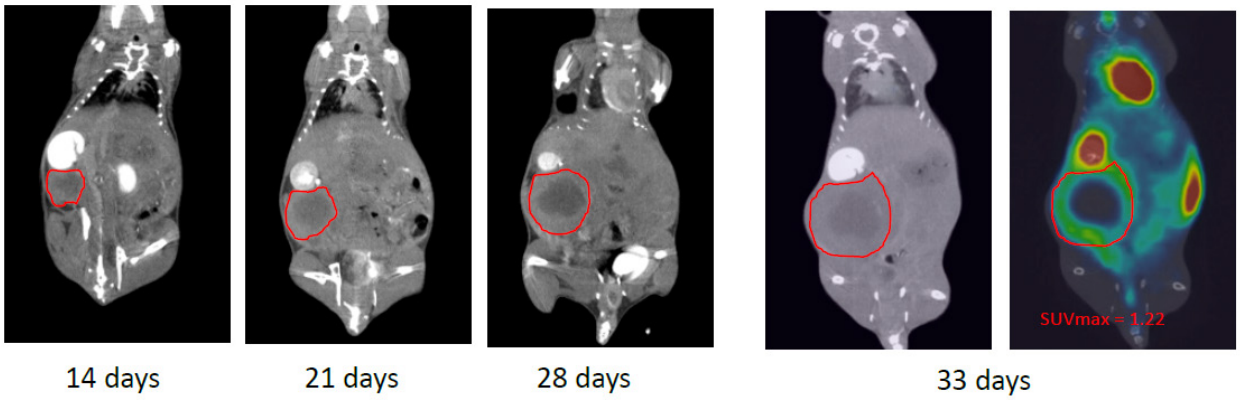

Figure 20: Representative orthotopic neuroblastoma tumor shown by contrast-enhanced CT and [18]F-FDG PET/CT. Days= time post implant.

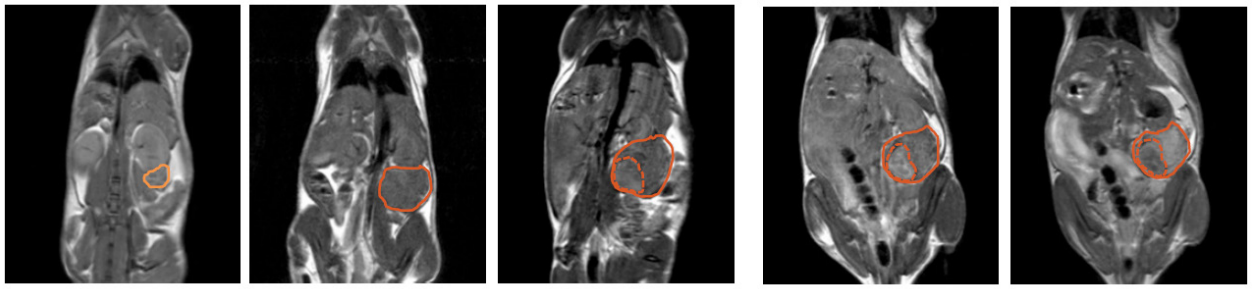

Figure 21: Representative orthotopic neuroblastoma tumor shown by T1W MRI. Days=time post implant.

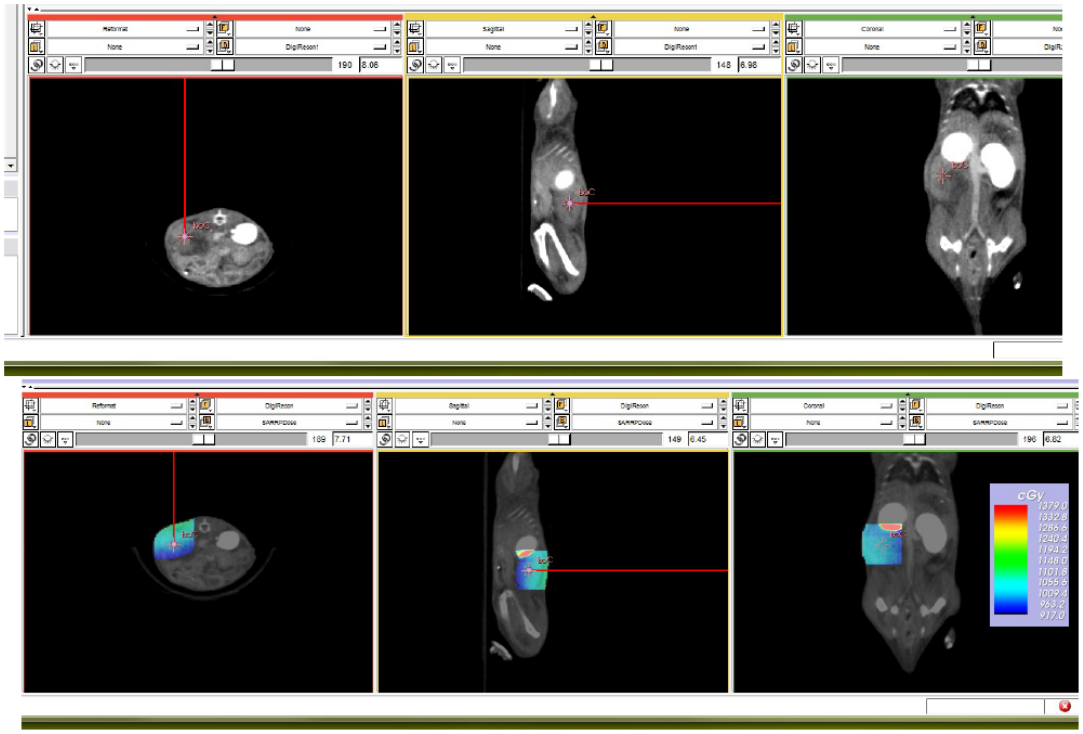

Figure 22: Screen-grabs from planning software using CT image guidance. Radiation dose is indicated by color map. Top: CT-image used to identify the tumor. Bottom: Dose distribution from planning software.

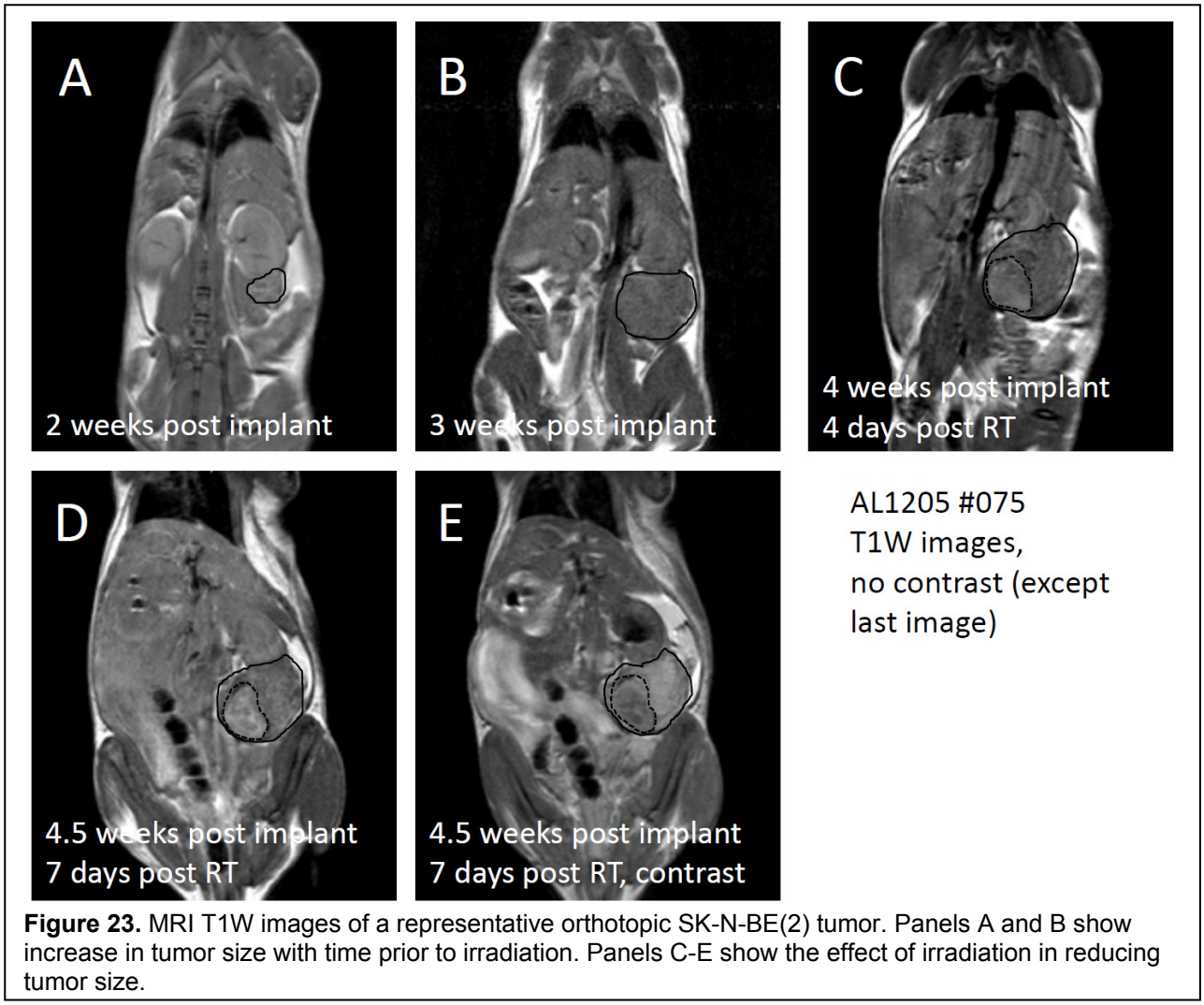

Figure 23. MRI T1W images of a representative orthotopic SK-N-BE(2) tumor. Panels A and B show increase in tumor size with time prior to irradiation. Panels C-E show the effect of irradiation in reducing tumor size.

Tumor histology indicated Ki-67 positive tumor cells (proliferating). However, antibody-specific immunohistochemistry of the orthotopic tumors did not detect changes in vascular parameters (CD34 tumor vessels, VEGF) between irradiated and non-irradiated tumors; this was an aim of SubTask2. The harvested orthotopic tumors were less solid than the subcutaneous tumors, and lost 3D architectural integrity during tumor sectioning (**Figure 23**). A representative image of an orthotopic tumor is shown in **Figure 24**.

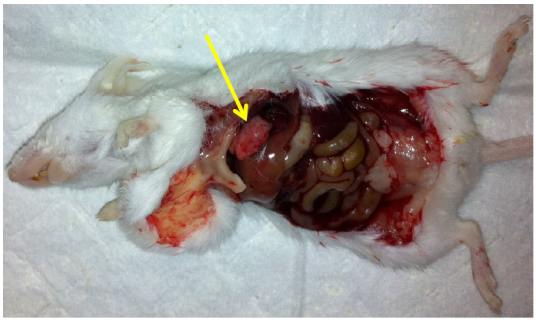

Figure 24. Representative orthotopic SK-N-BE(2) tumor grown in a CD17/SCID mouse. Tumor is visable above the liver but below the diaphragm (yellow arrow).

KEY RESEARCH ACCOMPLISHMENTS

Demonstrated differences in subcutaneous tumor response after PRT or SRT were not related to in vitro radiation response for three neuroblastoma cell lines. Of the three neuroblastoma cell lines investigated in vivo, differences between PRT and SRT were only evident for MYCN-amplified SK-N-BE(2) tumors. The effectiveness of PRT over SRT in SK-N-BE(2) tumors was dramatic.

Established subcutaneous and orthotopic tumor models for neuroblastoma.

Demonstrated that the degree of radiation-induced VEGF expression corresponded with tumor response to PRT and SRT. An increase in VEGF expression was seen after PRT in tissue culture (detected by ELISA in the culture medium) and in tissue histology as assessed by antibody specific immunohistochemistry.

Demonstrated that tumor immunohistochemistry after PRT or SRT suggested differential effects on tumor vasculature and hypoxic response (CA9, GLUT1 and VEGF) in subcutaneous tumors.

Demonstrated the response of subcutaneous tumors to PRT treatment may be important in tumor metastasis since a role for E-selectin was established.

REPORTABLE OUTCOMES

PRT may provide a new treatment for MYCN amplified neuroblastoma tumors, since SK-N-BE(2) tumors are radiosensitivity to pulsed treatment regimes.

CONCLUSION

Pulsed RT may be a benefit for a subset of neuroblastoma tumors that are MYCN amplified, and show low levels of radiation-induced VEGF expression.

These data are being prepared in a manuscript for submission to Cancer Research.

REFERENCES

1. Meitar, D., et al., Tumor angiogenesis correlates with metastatic disease, N-myc amplification, and poor outcome in human neuroblastoma. J Clin Oncol, 1996. 14(2): p. 405-14.
2. Canete, A., et al., Angiogenesis in neuroblastoma: relationship to survival and other prognostic factors in a cohort of neuroblastoma patients. J Clin Oncol, 2000. 18(1): p. 27-34.
3. Rossler, J., et al., Vascular endothelial growth factor expression in human neuroblastoma: up-regulation by hypoxia. Int J Cancer, 1999. 81(1): p. 113-7.
4. Yang, Q.W., et al., Methylation-associated silencing of the thrombospondin-1 gene in human neuroblastoma. Cancer Res, 2003. 63(19): p. 6299-310.
5. Breit, S., et al., The N-myc oncogene in human neuroblastoma cells: down-regulation of an angiogenesis inhibitor identified as activin A. Cancer Res, 2000. 60(16): p. 4596-601.
6. Breit, S., et al., N-myc down-regulates activin A. Biochem Biophys Res Commun, 2000. 274(2): p. 405-9.
7. Krueger, S.A., et al., Transition in survival from low-dose hyper-radiosensitivity to increased radioresistance is independent of activation of ATM Ser1981 activity. Int J Radiat Oncol Biol Phys, 2007. 69(4): p. 1262-71.
8. Marples, B. and M.C. Joiner, The response of Chinese hamster V79 cells to low radiation doses: evidence of enhanced sensitivity of the whole cell population. Radiat Res, 1993. 133(1): p. 41-51.
9. Schoenherr, D., et al., Determining if low dose hyper-radiosensitivity (HRS) can be exploited to provide a therapeutic advantage: a cell line study in four glioblastoma multiforme (GBM) cell lines. Int J Radiat Biol, 2013. 89(12): p. 1009-16.
10. Short, S.C., et al., Low-dose hypersensitivity after fractionated low-dose irradiation in vitro. Int J Radiat Biol, 2001. 77(6): p. 655-64.
11. Martin, L., et al., Recognition of O6MeG lesions by MGMT and mismatch repair proficiency may be a prerequisite for low-dose radiation hypersensitivity. Radiat Res, 2009. 172(4): p. 405-13.
12. Dilworth, J.T., et al., Pulsed low-dose irradiation of orthotopic glioblastoma multiforme (GBM) in a pre-clinical model: Effects on vascularization and tumor control. Radiother Oncol, 2013. 108(1): p. 149-54.
13. Lee, D.Y., et al., Pulsed versus conventional radiation therapy in combination with temozolomide in a murine orthotopic model of glioblastoma multiforme. Int J Radiat Oncol Biol Phys, 2013. 86(5): p. 978-85.
14. Park, S.S., et al., MicroPET/CT Imaging of an Orthotopic Model of Human Glioblastoma Multiforme and Evaluation of Pulsed Low-Dose Irradiation. Int J Radiat Oncol Biol Phys, 2011. 80(3): p. 885-92.
15. Schoenherr, D., et al., Determining if low dose hyper-radiosensitivity (HRS) can be exploited to provide a therapeutic advantage: A cell line study in four glioblastoma multiforme (GBM) cell lines. Int J Radiat Biol, 2013.
16. Krueger, S.A., et al., The effects of G2-phase enrichment and checkpoint abrogation on low-dose hyper-radiosensitivity. Int J Radiat Oncol Biol Phys, 2010. 77(5): p. 1509-17.
17. Krueger, S.A., et al., Role of apoptosis in low-dose hyper-radiosensitivity. Radiat Res, 2007. 167(3): p. 260-7.

APPENDICES

Work was presented at the 59th Radiation Research Society Annual Meeting in New Orleans. 9/15/2013 to 9/19/2013 as a research poster. Control/Tracking Number: 13-A-382-RRS

POSTER SESSION PS4-34: Wednesday 18th September 2013

Overcoming mechanisms of tumor radiation resistance: The use of low-dose pulsed radiotherapy.

Brian Marples, PhD; Sarah A. Krueger, PhD; Sandra Galoforo, MS; Diane Schoenherr, BS; Jonathan Kane, BS; and George D. Wilson, PhD,
William Beaumont Hospital, Royal Oak, MI

Patient survival for highly aggressive advanced-stage neuroblastoma remains poor despite a multidisciplinary approach involving aggressive surgery, chemotherapy and adjuvant radiotherapy (RT). The large RT treatment volume, and concerns about the proximity of radiosensitive normal structures, restricts the tumoricidal dose of radiotherapy that can be delivered which limits the effectiveness of adjuvant RT. To address this, we delivered radiotherapy using an entirely novel treatment schedule designed to minimize normal tissue damage. The concept was to deliver 10 pulses of low-dose RT (PRT, 10 x 0.2 Gy) using a 3 minute inter-pulse interval to introduce the RT-induced damage at a level that spares tumor vasculature in order to prevent the development of treatment-induced hypoxia, since this increases tumor resistance to radiation and chemotherapy. Moreover, damage produced at this dose level evades ATM dose-dependent DNA damage detection and repair mechanisms. In vitro clonogenic survival experiments demonstrated that a single dose of PRT was not inferior to a continuously delivered standard 2 Gy dose (SRT). PRT was delivered at 0.25 Gy/min and SRT at 0.69 Gy/min using a Faxitron 160 kVp animal X-irradiator (0.5 mm Cu and Al filters; HVL: 0.77 (mm CU)). Female CB-17/SCID mice were xenotransplanted subcutaneously in the flank at 6-8 weeks of age with either SK-N-SH, SK-N-BE or MCIXC neuroblastoma cells and the subsequent tumors irradiated with a total dose of 20 Gy given over 10 consecutive days (2 Gy/day) as either PRT or SRT. Tumor response was evaluated by physical measurements three times a week and by imaging using F18-FDG PET/CT 1 day prior to and 2 days post radiation treatment. For SK-N-BE tumors, significant differences in CT volume between PRT and SRT were evident at 5 days ($p=0.008$) and 21 days ($p=0.014$) post treatment, and animals reached endpoint criteria at 56 days after PRT compared with 43 days for SRT ($p=0.012$). Similar differences in response were seen between PRT and SRT for MC-IXC tumors. Studies with SK-N-SH are on-going. Quantitative immunohistochemistry identified differences in vascular density (CD34) and hypoxic markers (HIF1/CAXI) after PRT or SRT. These data indicate that PRT produces greater tumor control than SRT in this model. The work was funded by DOD PRMRP Award W81XWH-12-1-0355.

Overcoming mechanisms of tumor radiation resistance: The use of low-dose pulsed radiotherapy

Brian Marples§, Sarah A. Krueger, Sandra Galoforo, Diane Schoenherr, Jonathan Kane and George D. Wilson.

Department of Radiation Oncology.
William Beaumont Hospital, Royal Oak, MI.

Introduction

Neuroblastoma is the most common extra-cranial solid tumor of early childhood. Variable response is seen from spontaneous regression to highly aggressive disease which is resistant to multimodality treatment including conventionally delivered radiotherapy [1]. MYCN is amplified in 25% of tumors and is a genetic marker for treatment failure [2]. Tumor microvessel density [3, 4], angiogenic growth factor expression (*e.g.* VEGF) and down-regulation of angiogenic factors have been associated with advanced stage disease, along with apoptotic resistance owing to MYCN amplification [5, 6]. Therefore, novel approaches targeting tumor angiogenesis represent promising strategies for overcoming advanced disease. Our previous pre-clinical studies with glioblastoma multiforme (GBM) have demonstrated pulsed radiotherapy (PRT) offers a larger therapeutic benefit than continuously-delivered standard radiotherapy (SRT) [7-9]. In GBM, PRT spared tumor vasculature which maintained tumor oxygenation via a VEGF-based mechanism. Therefore, we hypothesized that PRT may be an effective treatment of neuroblastoma.

1. Maris et al., Lancet, 2007. 369(9579): p. 2106-20.
2. Maris, N Engl J Med, 2010. 362(23): p. 2202-11.
3. Meitar et al., J Clin Oncol, 1996. 14(2): p. 405-14.
4. Canete et al., J Clin Oncol, 2000. 18(1): p. 27-34.
5. Tweddle et al., Cancer Lett, 2003. 197(1-2): p. 93-8.
6. Brelt et al., Cancer Res, 2000. 60(16): p. 4596-601.
7. Dilworth et al., Radiother Oncol, 2013. 108(1): p. 149-54.
8. Lee et al., Int J Radiat Oncol Biol Phys, 2013. 86(5): p. 978-85.
9. Park et al., Int J Radiat Oncol Biol Phys, 2011. 80(3): p. 885-92.

Materials and methods

Neuroblastoma cells: SK-N-BE(2), SK-N-SH, MC-IXC, and SH-SY5Y cells were purchased from ATCC. SK-N-BE(2), MC-IXC and SH-SY5Y were grown in DMEM/F12 with 10% FBS and Pen/Strep. SK-N-SH cells were grown in DMEM with 10% FBS, Pen/Strep, L-glutamine, non-essential amino acids and sodium pyruvate. All cell lines were grown as monolayer cultures at 37°C in a 5% CO_2 incubator. SK-N-BE(2) cells are MYCN amplified, wild type ALK, with moderate levels of dopamine β hydroxylase activity. Conversely, SK-N-SH cells are not MYCN amplified have an ALK mutation (F1174L) and high levels of dopamine β hydroxylase activity. Doubling times: SK-N-BE(2)=35hr; SK-N-SH=75hr; SH-SY5Y=75hr; MC-IXC=30hr

Animals: The protocol was approved by the William Beaumont Hospital IACUC. Female CB17-SCID mice (Charles River, MA) were housed in conventional micro-isolator cages and given standard rodent chow and water ad libitum. 2x10-6 cells in 100 µL matrigel were implanted on the right rear flank or orthotopically.

Radiation schedule: Anesthetized animals were irradiated daily with 2-Gy, either by SRT (continuously delivered) or PRT (10 pulses of 0.2 Gy, separated by 3-minute intervals) to a total dose of 20 Gy over 10 consecutive days. RT was delivered using a Faxitron 160 kVp animal X-irradiator (0.5 mm Cu and Al filters; HVL: 0.77 (mm CU)) with a dose rate of 0.69 (Gy/min (SRT) or 0.25 Gy/min (PRT).

Tumor imaging and endpoint: Tumor volumes were determined by microPET/CT imaging and calipers. A FLEX Triumph™ combined small-animal PET/CT system (Gamma Medica-Ideas) was used for contrast-enhanced CT (80 kV/250 µA, 170 µl Omnipaque 350, GE Healthcare) and [18F]-FDG-PET (22.2 MBq ±10% in 200 µl in 30 secs). Tumor volume by caliper measurement was calculated using the standard formula (π/6)*a*b*b where a is the largest and b is the smallest diameter.

Cell Proliferation/MTT: 2,000-5,000 cells were plated into individual wells depending on cell type for MTT assays. Plates were irradiated with 2 Gy SRT, 10x0.2 Gy PRT or sham treated for five consecutive days.

VEGF Levels. VEGF levels were measured using a ELISA kit from R&D Systems.

Statistical analysis: Student t-test assuming unequal variances, with p values less than 0.05 considered biologically significant.

Histology: By Definiens Tissue Studio Software (DTSS). Regions of interest (ROI) were determined from the entire histology image. A DTSS solution was created by initializing cellular analysis, detecting marker areas, and classifying stain intensities as low, medium or high; and then applied to all ROI. The results are *marker area* and *percent area stained*, all divided amongst the low, medium, and high intensity.

Results

Figure 1: Radiation response as determined by MTT. No differences in response were seen between SRT and PRT. γH2A.X staining (DNA dsbs) are shown for SK-N-BE(2) and SK-N-SH.
Figure 2: *In vitro* VEGF expression by ELISA. SK-N-BE(2) had 3-fold higher levels of VEGF than SK-N-SH cells (p<0.001). SK-N-BE(2) and MC-IXC were comparable.
Figure 3: Fold increase in VEGF expression after 5 consecutive days of SRT or PRT. Significant increases were seen for SK-N-SH (p<0.001) and MC-IXC (p<0.05) cells.
Figure 4: Tumor regrowth delay as assayed by caliper measurements. The extent of growth delay corresponded with *in vitro* radiation response. SK-N-BE(2) tumors responded differently to PRT and SRT. For all three tumor types, the difference in tumor response to PRT and SRT corresponded with radiation-induced *in vitro* expression of VEGF.
Figure 5: Tumor response assayed by CT and PET. Responses after PRT or SRT were comparable.
Figure 6: Histological comparison of SK-N-BE(2) tumors. Differences in staining were evident between SRT and PRT treated tumors for E-Selectin, VEGF, CA9 and GLUT1.

§correspondence: brian.marples@beaumont.edu. Support: **DOD PRMRP Award W81XWH-12-1-0355**

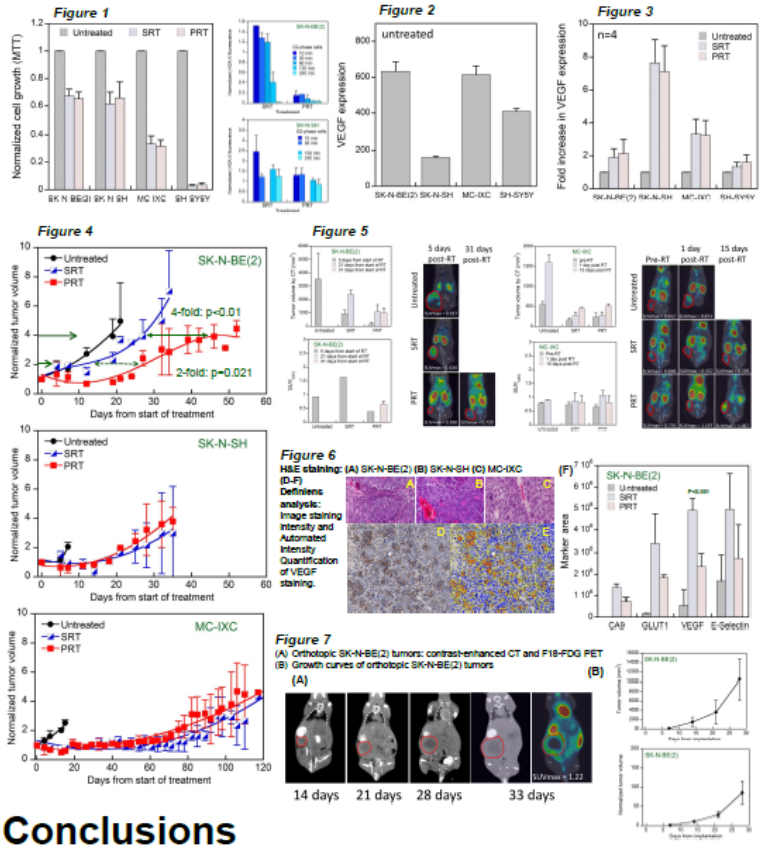

Conclusions

1. Differences in tumor response after PRT or SRT were not related to *in vitro* radiation response.
2. The degree of radiation-induced VEGF expression corresponded with tumor response to PRT or SRT (Figures 2-4, Figure 6).
3. Tumor immunohistochemistry after PRT or SRT suggested differential effects on tumor vasculature and hypoxic response (CA9, GLUT1 and VEGF: Figure 6). PRT response may be important in tumor metastasis (E-selectin; Figure 6).
4. These subcutaneous neuroblastoma studies are preliminary, and additional data are needed to confirm the therapeutic benefit of PRT. However, PRT may provide a new treatment for MYCN amplified tumors. An orthotopic tumor model is being used to address this question (Figure 7).

Work has been submitted and accepted to the American Society for Radiation Oncology (ASTRO) 56th Annual Meeting, September 14-17, 2014 (Moscone Center, San Francisco).The work as accepted as a research poster (Tracking Number: #: 2014-A-3240-ASTRO)

Evaluating Low-Dose Pulsed Radiotherapy in Murine Models of Neuroblastoma.

Sarah A. Krueger PhD, Diane Schoenherr BS, Sandra Galoforo MS, Mohamed Dabjan MD
George D. Wilson PhD and Brian Marples PhD
Department of Radiation Oncology, William Beaumont Hospital, Royal Oak, MI, USA

Objective/Purpose(s):
Highly aggressive advanced-stage neuroblastoma is treated with a multimodality approach but survival remains poor. The aim of this study was to evaluate low-dose pulsed radiotherapy (PRT) as a novel treatment for neuroblastoma. Although the mechanism of PRT is not fully elucidated, it is thought to induce DNA damage below the activation threshold of ATM-dependent DNA detection, repair and cell cycle checkpoint mechanisms, and also protect tumor vasculature.

Materials/Methods:
Radiosensitivity of SK-N-BE(2), SK-N-SH, MC-IXC, and SH-SY5Y neuroblastoma cells was determined by clonogenic assay. DNA repair was assessed by H2AX foci and apoptosis by caspase-3. Subcutaneous xenograft tumors were established from SK-N-SH, SK-N-BE(2), or MC-IXC cells in female CB-17/SCID mice and irradiated with a total dose of 20 Gy given over 10 consecutive days (2 Gy/day) as either continuously-delivered standard RT (SRT) or PRT (10 x 0.2 Gy using a 3 minute inter-pulse interval). Tumor response was evaluated 3 times a week by caliper measurements. F18-FDG PET/CT was also performed 1 day prior to and 2 days post RT. VEGF expression was assayed by ELISA. The study was approved by the Institutional IACUC.

Results:
In vitro, a single 2 Gy dose of PRT was not inferior to SRT in any of the 4 cell lines despite the prolonged delivery time. *In vivo*, PRT and SRT were equally effective at controlling MC-IXC and SK-N-SH subcutaneous tumors. However, significant differences in tumor volume and regrowth were evident for MYCN amplified SK-N-BE(2) tumors between PRT and SRT at 5 days (p=0.008) and 21 days (p=0.014) post treatment. Endpoint criteria was reached at 43 days for SRT but 56 days after PRT (p=0.012). Furthermore, tumors treated with PRT demonstrated a significant increase in FDG PET maximum standardized uptake value after treatment (SUVmax=1.13 SRT, 1.79 PRT, p=0.03). This increase was also significant when compared to pre-treatment values for PRT (SUVmax PreTreatment = 1.04, p=0.009). Quantitative immunohistochemistry identified differences in vascular density (CD34) and hypoxic markers (HIF1/CA-IX) between PRT and SRT. VEGF levels in the blood did not change after PRT tumor irradiation but increased after SRT.

Conclusion:
These data indicate that PRT may provide a new treatment regimen for MYCN amplified neuroblastoma. While the exact mechanism behind PRT is not known, changes in vascularity and cellular proliferation during treatment likely play vital roles. These data are currently being confirmed in an orthotopic SK-N-BE(2) model utilizing non-invasive PET imaging.

Funded by DOD PRMRP Award W81XWH-12-1-0355.